

GRB 050502B optical afterglow: a jet break at high redshift[★]

P. Afonso¹, J. Greiner¹, E. Pian^{2,3,4}, S. Covino⁵, D. Malesani⁶, A. Küpcü Yoldaş⁴, T. Krühler^{1,7}, C. Clemens¹, S. McBreen^{1,8}, A. Rau¹, D. Giannios⁹, and J. Hjorth⁶

¹ Max-Planck-Institut für extraterrestrische Physik, Giessenbachstraße 1, 85748 Garching, Germany

² Osservatorio Astronomico di Trieste, Istituto Nazionale di Astrofisica, Via G.B. Tiepolo 11, 34131 Trieste, Italy

³ Scuola Normale Superiore, Piazza dei Cavalieri 7, 56126 Pisa, Italy

⁴ European Southern Observatory, Karl-Schwarzschild-Straße 2, 85748 Garching, Germany

⁵ Osservatorio Astronomico di Brera, Istituto Nazionale di Astrofisica, Via Brera 28, 20121 Milano, Italy

⁶ Dark Cosmology Centre, Niels Bohr Institute, University of Copenhagen, Juliane Maries Vej 30, 2100 Copenhagen Ø, Denmark

⁷ Universe Cluster, Technische Universität München, Boltzmannstraße 2, 85748 Garching, Germany

⁸ University College of Dublin, Science Centre, School of Physics, Belfield, Dublin 4, Ireland

⁹ Princeton University, Department of Astrophysical Sciences, Peyton Hall, Princeton, NJ 08544-1001, USA

ABSTRACT

Aims. GRB 050502B is well known for the very bright flare displayed in its X-ray light curve. Despite extensive studies, however, the optical light curve has never been discussed and its redshift is unconstrained. Possible correlations between optical and X-ray data are analysed.

Methods. Photometric data from TNG in the *R* and *I* bands were used to compare the optical afterglow with the X-ray light curve. The *HyperZ* package and a late time VLT host observation were used to derive redshift estimates.

Results. The *I*-band afterglow decay followed a power-law of index $\alpha = 2.1 \pm 0.6$, after a late break at $\sim 1.3 \times 10^5$ s. The *R* – *I* color is remarkably red and the broadband spectral index $\beta_{\text{OX}} = 0.9 \pm 0.1$ is consistent with the X-ray spectral slope β_{X} . Although a photometric redshift of $z > 4$ is the most conservative result to consider, a photometric redshift of $z = 5.2 \pm 0.3$ is suggested with no extinction in the host, based on which an isotropic energy $E_{\gamma,\text{iso}} = (3.8 \pm 0.7) \times 10^{52}$ erg and a jet opening angle $\theta \sim 3.7^\circ$ are subsequently derived.

Conclusions. The combined X-ray and optical data suggest an achromatic break, which we interpret as a jet break. The post jet break slope obeys roughly the closure relation for the jet slow cooling model. Because of the afterglow’s very red color, in order for the redshift to be low ($z < 1$), extinction, if present in the host, must be significantly high. Since the optical-to-X-ray index is consistent with the X-ray spectrum, and there is no XRT evidence for excess N_{H} , GRB 050502B was likely at high redshift.

Key words. Gamma rays: bursts, observations: individual: GRB 050502B

1. Introduction

The gamma-ray burst (GRB) 050502B was a remarkable event showing a conspicuous X-ray flare lasting from ~ 400 to 1400 s after trigger, with as much energy ($\sim 9 \times 10^{-7}$ erg cm^{-2} , in the 0.3–10.0 keV band) as the prompt emission itself [$(8.0 \pm 1.0) \times 10^{-7}$ erg cm^{-2} , in the 15–350 keV band]. The X-ray light curve also showed later activity and a second less intense flare, followed by a possible jet break at $\sim 1.1 \times 10^5$ s (Falcone et al. 2006; Burrows et al. 2005b). Given the exceptionality of this GRB, it is important to study its optical afterglow, searching for properties that may lead to a better understanding of its phenomenology.

As expected, when the relativistic jet slows down, the aberration of light due to Special Relativity effects becomes less important, and thus the beaming angle, $\theta_b \sim 1/\Gamma$, increases within the jet (Rhoads 1997). A jet break occurs when the Lorentz factor is such that $1/\Gamma > \theta_{\text{jet}}$, resulting in a significant decrease of the afterglow brightness and steepening of the light curve at all

wavelengths. In the *Swift* satellite era (Gehrels et al. 2004), X-ray light curves are much better sampled than previously, but simultaneous optical and X-ray light curve breaks have been rarely observed. For example, from the sample of Liang et al. (2008), with *Swift* X-Ray Telescope (XRT; Burrows et al. 2005a) data for 179 GRBs and 57 pre- and post-*Swift* GRBs optical afterglow data, only 7 of them show an achromatic break. This apparent lack of jet breaks is still in debate and could be due to a combination of higher redshifts, fainter bursts, larger opening angles, etc. Models that go beyond the fireball external shock afterglow scenario have also been explored, as they include an extra component that can be described as “late prompt” emission due to late time activity of long living central engines. As discussed by Ghisellini et al. (2009) and Nardini et al. (2009), the lack of achromatic breaks could be explained by the presence of the “late prompt” emission.

The analysis of GRB 050502B optical data from the 3.58 m Telescopio Nazionale Galileo (TNG) was done with focus on correlations between the optical and X-ray afterglow behavior. In the next pages the X-ray light curve is discussed first, following Falcone et al. (2006) as a guideline. Evidence for a jet break and large redshift are presented later in § 3.

Send offprint requests to: P. Afonso, e-mail: pafonso@mpe.mpg.de

[★] Based on observations made with the Italian Telescopio Nazionale Galileo (TNG) operated on the island of La Palma by the Fundación Galileo Galilei of the INAF (Istituto Nazionale di Astrofisica) at the Spanish Observatorio del Roque de los Muchachos of the Instituto de Astrofísica de Canarias (program AOT11-59) and with ESO Telescopes at the La Silla Paranal Observatories under program ID 177.A-0591.

2. Observations and data reduction

2.1. Optical data from TNG and VLT

At 09:25:40 UT, the Swift Burst Alert Telescope (BAT; Barthelmy et al. 2005) triggered and located GRB050502B (Pagani et al. 2005). The XRT repository indicates that the afterglow of GRB 050502B was observed at the coordinates RA = 09:30:10.11, Dec = +16:59:47.9 (J2000.0), being located within the XRT UVOT-enhanced position 1.4 arcsecond radius error circle. The detailed TNG *I* and *R* bands data, taken on 2005, May 3, 4 and 5 (1, 2 and 3 days after the trigger, respectively), are summarized in Table 1. Raw images were corrected for bad pixels, debiased and flat-fielded in a standard way with IRAF (Tody 1993). In addition, the TNG *I*-band images severely affected by fringing were corrected using standard routines. Photometry was done also with IRAF, using the USNO-B1.0 catalog for calibration purposes, which has a systematic error of ± 0.2 mag. In order to calibrate the afterglow photometry, 40 to 50 stars were used per final science image. The TNG photometric uncertainties listed in Table 1 are statistical only. Later in time the Sloan Digital Sky Survey (SDSS) Data Release 6, finally covered the field of view of GRB 050502B. A cross-calibration between USNO-B1.0 and SDSS catalogs yielded consistent zero points. Conversion from *r* to *R*-band and *i* to *I*-band was performed using observations of Landolt standard stars (Landolt 1992) in SDSS fields, following Chonis & Gaskell (2008).

To compute the flux density for the *R* and *I* bands, Vega flux reference values, f_0 , were taken from Fukugita et al. (1995). The correction for Galactic extinction was based on the interstellar extinction curves derived by Cardelli et al. (1989) and O'Donnell (1994), with $E(B - V) = 0.03$ mag (Schlegel et al. 1998).

Afterglow spectroscopy was attempted at the European Southern Observatory (ESO) Very Large Telescope (VLT), but unluckily the weather conditions did not allow for meaningful observations. Finally, late-time observations of the field of GRB 050502B were taken in the *R*-band with the Focal Reducer and Spectrograph 2 (FORs2) instrument at VLT, within the large program on GRB host galaxies (177.A-0591; PI: Hjorth). Observations were carried out 321 days after the GRB (on March 23, 2006), for a total exposure time of 2000 s. At the afterglow position, no object is detected down to a 3σ limiting magnitude of $R > 26$ mag.

2.2. Other optical data and upper limits

All published optical data are presented in Table 1. These include several upper limits (ULs) and in particular one more detection further to those by TNG, reported by the Australian National University (ANU) 1-m telescope (Rich et al. 2005a; Cenko et al. 2005). Unfortunately the ANU data were lost on a corrupted disk, being impossible to produce further refined photometry to include in this paper (B. Schmidt, personal communication).

During the giant X-ray flare, the *Swift*-Ultraviolet and Optical Telescope (UVOT; Roming et al. 2005) did not detect any optical counterpart, reporting only UL for a 9×10 s exposure (Schady et al. 2005). The UVOT repository (Roming et al. 2009) gives a detailed sequence of observation times, as each of the *UBV* filters was used, and more than the initial 9×10 s exposure were taken. The time error bars in Fig. 1 reflect these data. For the time period of the X-ray flare, observations with the *U* filter started 192 s after the burst, ending 960 s after, with interruptions to switch to other filters. For the *V* and *B* filters the start

Table 1. Data from TNG and other telescopes taken from the literature. The first column gives the mid time or the start of observations. For the ART and Himalayan telescopes data, the UL calibration catalog was not mentioned; thus Vega magnitudes were assumed and converted to AB magnitudes here.

Time (s)	Filter	Telescope	Exposure (s)	Magnitude (AB)
56.7	<i>B</i>	Ashra 0.3m ^a	1.4	> 15.9
56.7	<i>R</i>	Ashra 0.3m ^a	1.4	> 14.7
180	<i>B</i>	Ashra 0.3m ^a	25 × 4	> 18.2
180	<i>R</i>	Ashra 0.3m ^a	25 × 4	> 17.1
576	<i>U</i>	UVOT ^b	9 × 10	> 19.7
577	<i>V</i>	UVOT ^b	9 × 10	> 18.4
633	<i>B</i>	UVOT ^b	9 × 10	> 19.1
570	<i>V</i>	ANU 1m ^{c,d,e}	not given	> 20.6
900	<i>V</i>	ANU 1m ^{c,d,e}	not given	> 20.1
1080	<i>V</i>	ANU 1m ^{c,d,e}	not given	> 20.7
1200	<i>V</i>	ANU 1m ^{c,d,e}	not given	> 21.7
3950	<i>I</i>	ANU 1m ^{c,d,e}	total ~ 4020	20.23 ± 0.09
7339	<i>I_c</i>	ART 0.36m ^f	87 × 60	> 18.9
15560	<i>R</i>	Lulin 1m ^g	not given	> 21.9
19160	<i>R</i>	Himalayan 2m ^h	4 × 600	> 22.6
22566	<i>V</i>	Aries 1m ⁱ	12 × 300	> 21.4
128796	<i>I</i>	TNG	60	21.73 ± 0.21
129104	<i>I</i>	TNG	300	21.28 ± 0.08
129521	<i>I</i>	TNG	300	21.15 ± 0.07
157680	<i>i</i>	P60 ^c	10 × 120	> 21.3
215661	<i>R</i>	TNG	11 × 300	23.71 ± 0.20
219235	<i>I</i>	TNG	2 × 300	22.59 ± 0.12
302676	<i>I</i>	TNG	8 × 300	> 23.7
~ 2.8 × 10 ⁷	<i>R</i>	VLT	2000	> 26

^aSasaki et al. (2005), ^bSchady et al. (2005), ^cCenko et al. (2005), ^dRich et al. (2005a), ^eRich et al. (2005b), ^fTorii (2005), ^gSanchawala et al. (2005), ^hBhatt et al. (2005), ⁱMisra & Pandey (2005).

and end times are 234-920 s and 290-975 s, respectively. Table 1 indicates the median times for these UVOT observations. Several subsequent UVOT observations, roughly following the timing of XRT exposures, continued late after the flare but resulted only in shallow upper limits (not reported in Table 1).

3. Results

3.1. Optical and X-ray light curves: the jet break

To produce the X-ray light curve shown in Fig. 1, in order to compute the X-ray flux densities at 1 keV, the unabsorbed flux integral was computed over the energy range 0.3-10 keV. The required spectral indices β are fitted for the window timing (WT) and photon counting (PC) XRT modes and taken from the *Swift*-XRT spectrum repository (Evans et al. 2007).

The main feature of the XRT light curve is a giant flare that occurs on top of an underlying decaying afterglow, obeying a power-law $F(t) \propto t^{-\alpha}$ of time index $\alpha = 0.8 \pm 0.2$. Though not shown anymore in the current light curve found in the XRT repository, Falcone et al. (2006) report for their binned data that the pre-flare decay rate is maintained in the post-flare, up until to $\sim 10^4$ s after the GRB start time. The light curve then exhibits a flattening combined with two over-imposed rebrightenings at $\approx 3 \times 10^4$ and $\approx 8 \times 10^4$ s, respectively. The latter marks the onset of a steep decline, which could be a jet break. From the shallow

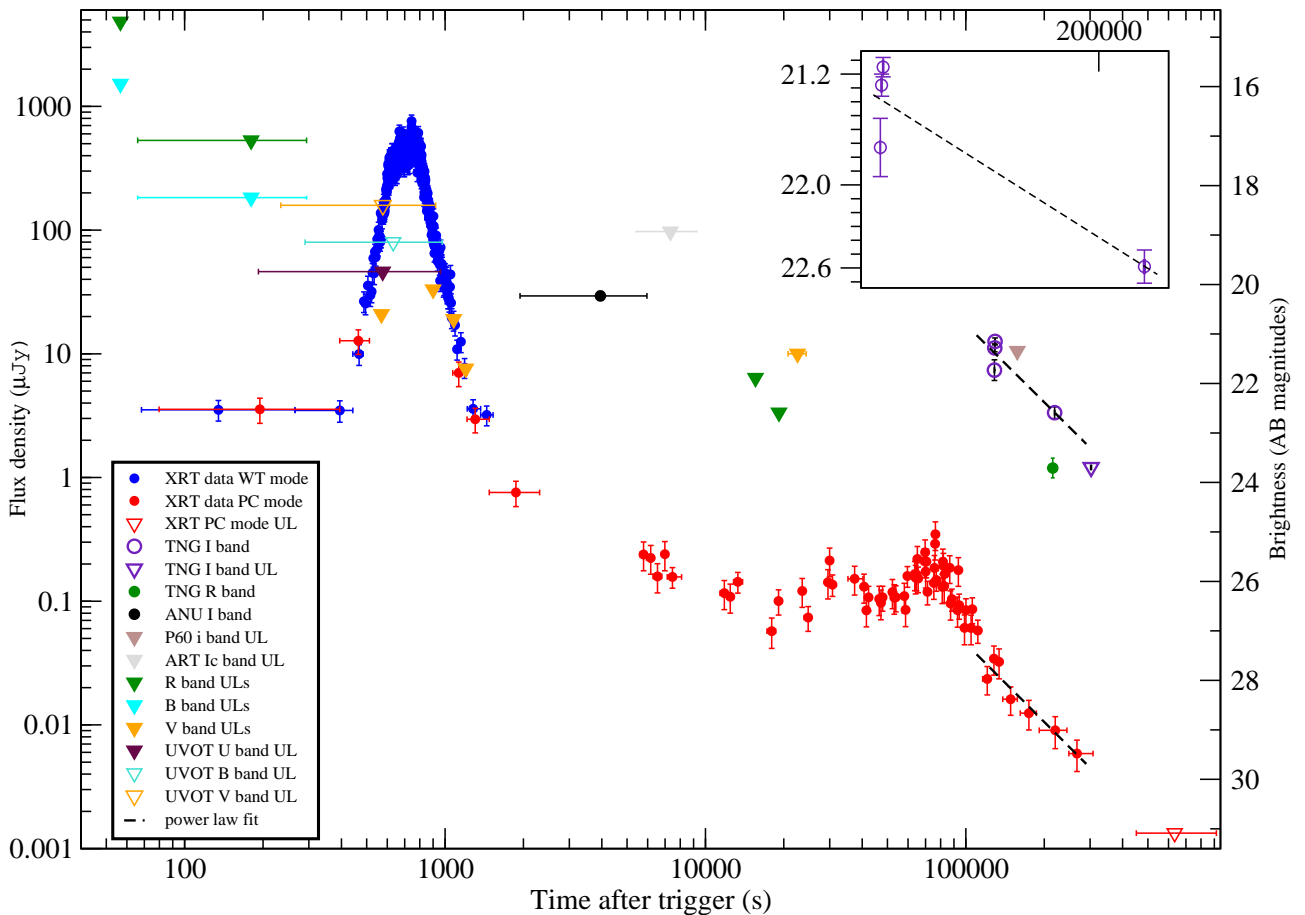


Fig. 1. Optical and X-ray (1 keV) light curves. Horizontal error bars represent the exposure times. Dashed lines represent the time power-law fits to the 4 TNG *I*-band detections and to the last 7 X-ray data points. The inserted box zooms in on the TNG *I*-band detections.

decay phase the light curve evolves directly into post-jet break, not showing the less steep pre-jet break phase (Panaiteescu 2006).

Considering the available *I*-band data at a time $t > 1.28 \times 10^5$ s, when fitted with a power-law, the time decay index is $\alpha = 2.1 \pm 0.6$. This late time decay must be a post-break decay, since the ANU telescope detection appears to constrain the early time decay to a slope shallower than that of the TNG.

When fitting the last seven X-ray time bins with a power-law, the result is $\alpha = 2.1 \pm 0.3$. The first of these seven bins matches the start of our optical observations at $\sim 1.28 \times 10^5$ s. If considering one extra earlier bin, i.e., for $t > 1.1 \times 10^5$ s (like in Falcone et al. 2006), the time index is then $\alpha = 2.3 \pm 0.3$, while Falcone et al. (2006) got a power-law time index of $\alpha = 2.8 \pm 0.8$.

The results presented in this work are compatible with those from Falcone et al. (2006), despite using a slightly different X-ray data binning. From the currently available *Swift*-XRT data repository, it can be established that for the last seven bins the count rate light curve has a minimum of 17 and a maximum of 99 counts per bin. Thus such binning is statistically meaningful.

Noting that the steep optical decay overlaps in time and has a time index consistent (within errors) with that in the X-rays, the data suggest thus a jet break.

The spectral index in any given band across a jet break should be unchanged. Therefore, in order to test the jet break hypothesis, an averaged spectrum was created in the *Swift*-XRT repository for all points with $t > 1.1 \times 10^5$ s, resulting in a spec-

tral index of $\beta_X = 1.0^{+0.4}_{-0.2}$, with a best fit value in excess of the Galactic hydrogen column density of $N_H = 0^{+3.7}_{-0} \times 10^{20} \text{ cm}^{-2}$. For the interval $[\sim 1000, 200000]$ s, the spectral index is basically the same, with $\beta_X = 1.0^{+0.3}_{-0.2}$.

3.2. The Spectral Energy Distribution

The broadband spectral energy distribution (SED) was computed at the epoch of our single *R*-band detection. Since the *R*-band point precedes the closest *I*-band point by ~ 1 hr, the *I*-band post-jet break slope was used to extrapolate the *I*-band value (0.04 magnitudes brighter) at the *R*-band observation time. The effective wavelengths, λ_0 , corresponding to the *R* and *I* bands, were taken from Fukugita et al. (1995). The X-ray data point used in the SED has a flux density (at 1 keV) of $9 \times 10^{-3} \mu\text{Jy}$, at the time of the penultimate bin point in the X-ray light curve. This X-ray bin point matches the extrapolated *I*-band and observed *R*-band observation time.

Fitting the broadband SED with a simple $F_\nu(\nu) \propto \nu^{-\beta}$ power-law yields a spectral index $\beta_{\text{OX}} = 0.9 \pm 0.1$. This value is consistent with the X-ray spectral index (§ 3.1), thus there is no indication of a break between the optical and X-ray spectra and the SED between the *I*-band and ~ 5 keV is well described by a single power-law with $\beta_{\text{OX}} = 0.9 \pm 0.1$.

Finally, although there is only one epoch at which the broadband SED could be computed, the temporal decay indices in the optical and X-rays are consistent as well, which is a necessary

condition to keep having β_X consistent with β_{OX} in other epochs. In fact if the optical and X-ray decay indices become different, it would imply necessarily a spectral break between optical and X-rays.

3.3. The closure relations

Considering the fireball synchrotron shock model as the major radiation mechanism responsible for the afterglows (e.g., Zhang & Mészáros 2004) and following, e.g., Sari et al. (1998), GRB 050502B roughly obeys the closure relations for a model of a uniform jet (valid for both ISM and wind cases) in a typical slow cooling regime, for $\nu > \nu_c$, where ν_c is the synchrotron cooling frequency. The electron power-law index, p , is deduced from the temporal decay index at the post-jet break phase, i.e., $F_\nu \propto t^{-p}$. Thus for $p \sim 2.1$ and $\beta_{OX} = 0.9 \pm 0.1$, within errors, it is observed $\alpha = 2\beta$.

3.4. Photometric redshift

The quasi-simultaneous R and I bands TNG observations at 215.6 and 219.2 ks, respectively, result in $R-I = 1.12 \pm 0.23$ mag. The correction for simultaneity (using the time index computed for the I -band) is smaller than the error due to the uncertainty in the photometry, resulting in $R-I = (1.16 \pm 0.23)$ mag. This very red color hints for either high redshift or high extinction in the host, or both. These possibilities were explored using the *HyperZ* photometric redshift code from Bolzonella et al. (2000). No reddening in the host and a fixed $\beta_{OX} = 0.9 \pm 0.1$ produce the best fitting result of $z = 5.2 \pm 0.3$ (see Fig. 2). Since β_{OX} and β_X are consistent, this further favors the unextinguished model.

3.5. Burst energetics

According to Cummings et al. (2005) the fluence in the BAT range (15-350 keV) is $F_\gamma = (8.0 \pm 1.0) \times 10^{-7}$ erg cm $^{-2}$. To estimate the energy of the burst if occurring at $z = 5.2$, the corresponding luminosity distance is computed in a concordance cosmology model (Spergel et al. 2003). With $H_0 = 71$ km s $^{-1}$ Mpc $^{-1}$, $\Omega_M = 0.27$ and $\Omega_\Lambda = 0.73$, it results $D_L = 49.84$ Gpc. For the BAT range of energies, considering the errors in the fluence and redshift, this results in an isotropic-equivalent energy of $E_{\gamma,iso} = 4\pi D_L^2 F_\gamma (1+z)^{-1} = (3.8 \pm 0.7) \times 10^{52}$ erg, which is a typical value for long GRBs.

The jet opening angle θ , which is dependent on the redshift and jet break time, can also be computed. To compare our results with $\theta \sim 8.1^\circ$ from Falcone et al. (2006), the same formula is followed, other than a small correction, required for dimensionality consistency, where $n_0 = n_{ism}/(1 \text{ cm}^{-3})$. Thus where Falcone et al. (2006) assumed $z = 1$ and $E_{52} = 1$, in $\theta = 7.8^\circ t_5^{3/8} E_{52}^{-1/8} n_0^{1/8} [(1+z)/2]^{-3/8}$, it is now $t_5 = 1.1$, for a jet break time of $\sim 1.1 \times 10^5$ s, $E_{52} = 3.8\eta_\gamma$, $n_0 \sim 1$, for a uniform external interstellar medium density, and $z = 5.2$; this gives $\theta \sim 3.7^\circ$. Note that, as in other works (e.g., Ghirlanda et al. 2007; Frail et al. 2001), $\eta_\gamma = 0.2$ corresponds to an assumed radiative efficiency of 20%. Given that the bolometric $E_{\gamma,iso}$ must be larger than that observed within the BAT range used here, $\theta \sim 3.7^\circ$ is thus an upper limit, within the typically observed jet opening angles (Ghirlanda et al. 2007).

4. Discussion

4.1. Optical and X-ray light curves: the jet break

The second and last bump on the X-ray light curve masks the true start of the jet break, while in the optical a possible bump or small flare cannot be ruled out. There is a small increase in brightness in the first three I -band data points, but it is not significant given that the first point does not have the best S/N. Also the second and third I -band data points are consistent, within errors, with no flaring, as can be better seen in the zoomed inserted box in Fig. 1. In any case even if this was a flare, in order to explain the rapid decay from the first 3 detections in May 3 (starting at 128 796 s after the trigger) to the following detection in May 4 (at 219 235 s), occurring simultaneously in the X-rays, the jet break still seems the best answer.

It is interesting to compare the last X-ray bump with the complex light curve of GRB 071010A (Covino et al. 2008), where after a rebrightening at 0.6 days after the trigger, a steeper decay began both in the X-ray and optical, as evidence of a jet break. In this and other GRBs with similar light curves, there is no plateau phase prior to the bump though - and rebrightening explanations related to the density profile of the circumburst medium have been invoked (among others).

The optical post-jet break slope could have been further constrained if earlier data had been taken, since the fitting of the X-ray jet break data points starts some ~ 33 min (2000 s) earlier than our first optical data point. Note also that the TNG I -band non-detection at the significance of 2σ (i.e., the UL of May 5, 2005, at ~ 302 ks post-burst) favors an even steeper post-jet break.

4.2. Photometric redshift

When considering extinction in the host, with data from only two filters, it is impossible to strongly constrain both the redshift and A_V , given that they are generically anticorrelated, as shown in Fig. 2. Several host extinction models were used with *HyperZ* and in Fig. 2 the Small Magellanic Cloud (SMC) model is shown as an example to illustrate the dependence with redshift. This suggests that a low redshift is allowed for large A_V values.

As noted by Falcone et al. (2006), during the observations the total N_H can be considered constant at approximately the Dickey & Lockman (1990) value for the Galactic hydrogen column density, $N_H = 3.6 \times 10^{20}$ cm $^{-2}$. Constructed with data from the XRT repository, a time-averaged spectrum between $T_0 + 68$ and $\sim 1.4 \times 10^5$ s is best fitted (assuming $z = 0$) with an absorbed power-law model where $N_H = 8.2_{-8.2}^{+20.6} \times 10^{19}$ cm $^{-2}$. This is a typical intrinsic excess value, similar to those observed in the high-redshift GRBs sample of Grupe et al. (2007). Within the XRT fit error this result is consistent with zero, but taking the upper error value allows to compute an upper limit on the possible excess extinction.

There is no exactly known relation between A_V and N_H in GRB environments. To find the dependence of the A_V ULs with z , the X-ray spectral fitting package *Xspec* (Arnaud 1996) was used, placing the excess N_H column at redshifts of 0, 1, 2, 3, 4 and 5. The cubic polynomial that represents the XRT UL curve in Fig. 2 fits the data points obtained from the Milky Way based Predehl & Schmitt (1995) relation, where $N_H = 1.79 A_V \times 10^{21}$ cm $^{-2}$. Although, in general, high N_H corresponds to high A_V , the dust-to-gas ratio in GRB hosts can be different and normally is smaller than in the Milky Way. Galama & Wijers (2001) report some examples with high N_H but with A_V being 10-100

times smaller than expected. Likewise the sample of Stratta et al. (2004) favors a dust-to-gas ratio of $\sim 1/10$ that of the Milky Way, as in a SMC environment. Therefore a more reasonable approach was to scale down by a factor of 10 the XRT UL data points presented in Fig. 2, after being computed from the Predehl & Schmitt (1995) relation.

Stressing that all the *Xspec* results are compatible with zero extinction, an inspection of Fig. 2, e.g., for $z = 4$ at the 1σ level, shows nevertheless an UL of $A_V \sim 0.5$ mag. This is a relatively high extinction, that cannot be probed directly at the rest frame by XRT, due to its spectral coverage. So a combination of both high redshift and A_V can also not be excluded and a more conservative result of $z > 4$ should be considered.

The GRB A_V distribution is poorly constrained. While in the past samples were biased towards low extinction bursts, showing typical intrinsic reddening to be well below $A_V \sim 0.5$ mag (Kann et al. 2006), recent observations provide evidence for highly reddened afterglows (Watson et al. 2006; Rol et al. 2007; Krühler et al. 2008; Elíasdóttir et al. 2009; Prochaska et al. 2009). The case of GRB 070306, detected initially in the *K*-band, is a remarkable example of a highly reddened burst with $z = 1.496$ and suggested $A_V = 5.6$ mag (Jaunsen et al. 2008). Tanvir et al. (2008) report GRB 060923A as being another similar extreme case.

As an additional note, since dust affects mostly the rest frame UV, normally a somewhat higher redshift ($\sim 2 - 3$) is needed in order to get such $R - I$ red color. Furthermore in the sample of Schady et al. (2007) all highly reddened bursts due to intrinsic extinction have large N_H in the XRT data, which is the opposite of the present case.

For $z > 4.5$, UVOT cannot detect anymore the Lyman limit (Roming et al. 2005) and the UVOT data do not indicate the presence of a strong rebrightening in the optical simultaneous to the giant X-ray flare. Note however that, independent of its origin, the very red color only strictly suggests very little flux in the blue and UV bands probed by UVOT, hence the occurrence of a dimmer optical flare cannot be totally excluded.

If allowing for the possibility that there is no correlation between A_V and N_H (e.g., Jakobsson et al. 2006, Watson et al. 2007), the constraint from the X-ray spectrum could be circumvented. In this case, however, the extinction corrected optical fluxes would be increasingly above the 0.9 power-law extrapolation from the X-ray band, thus producing a convex SED. Such an SED shape has not been proposed within any afterglow model, was never observed and seems therefore an extremely unlikely option.

Regarding the *R*-band VLT data, since GRB host galaxies can be very faint (e.g. Le Flocc’h et al. 2003) the VLT non-detection of a host galaxy provides only a mild limit on the redshift. It is difficult to quantify a lower limit given the scarcity of data, but looking into samples of GRB host galaxies, as in those of Wainwright et al. (2007) and Savaglio et al. (2009), hosts with magnitude $R \gtrsim 26$ typically have $z \gtrsim 1.5$. This can be taken as a rough lower limit to the redshift of GRB 050502B (Malesani et al. 2009).

4.3. Burst energetics

In § 3.5, $E_{\gamma,iso}$ was computed for $z = 5.2$. Just for reference, if taking $z = 1$, then $E_{\gamma,iso} = 2.1 \times 10^{51}$ erg, which compared to samples of other bursts with known redshift (e.g., Amati et al. 2008), would put GRB 050502B to the lower energy end of GRBs.

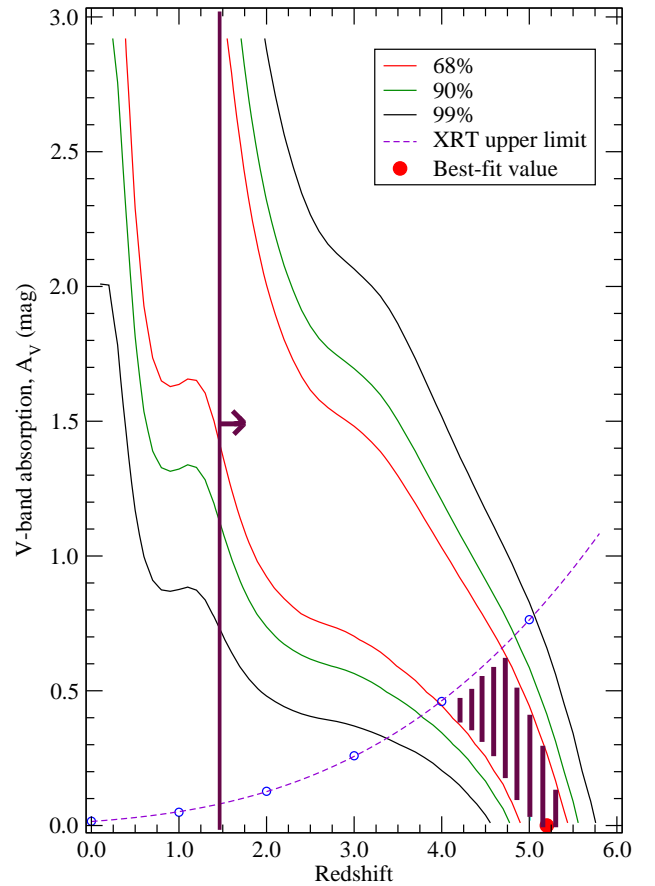


Fig. 2. Intrinsic reddening vs. redshift dependence, for an SMC extinction curve with SED slope fixed to $\beta = 0.9$. The 68%, 90% and 99% confidence contours are plotted. The XRT-fit line represents the A_V upper limits, converted as described in the text. The fit errors are, though, compatible with zero intrinsic N_H . The maroon shaded area represents the 1σ region of the contour plot constrained by the XRT upper limits. The vertical line at $z = 1.5$ represents the VLT lower limit due to the lack of a host detection.

A hard question to answer is how to compute a bolometric rest frame isotropic-equivalent energy with a proper k-correction without knowing exactly the value of the peak energy, E_p . Following Cummings et al. (2005) and Sakamoto et al. (2008), the BAT spectrum (range 15-350 keV) is well fitted by a single power-law with a photon index $\Gamma = 1.59 \pm 0.14$. From the BAT spectrum, ~ 90 keV is roughly the highest energy at which a reasonable detection still occurs and, given the value of Γ , this could be assumed as a lower limit for E_p . An empiric estimator could be considered instead, as in Sakamoto et al. (2009), where $\log(E_p/1 \text{ keV}) = 3.258 - 0.829 \Gamma$. Combining the estimator’s own 1σ uncertainties and those in Γ , results then in $E_p = 85^{+184}_{-52}$ keV. Taking $z = 5.2, 2.5$ and Γ as the high and low energy indices, respectively, of a Band function spectral shape (Band et al. 1993), if considering only the uncertainties in Γ , results already in a large ~ 200 keV uncertainty range for the rest frame peak energy, $E_{p,i} = 530^{+110}_{-90}$ keV. These estimators are only valid for BAT spectra that can be fitted by a single power-law, but older empiric estimators produce significantly different results (e.g. Liang et al. 2007).

In order to check if GRB 050502B obeys the Amati and Ghirlanda relations, the “standard” isotropic-equivalent bolometric energy release in the rest frame range of 1 keV to 10

MeV needs to be computed. It is difficult to reach firm conclusions given the errors in F_γ , Γ , z and the uncertainties in E_p and in the Band function indices. In a time dilation and k-correction computation (Amati et al. 2002), different combinations of parameters produce significantly different results. For reference, an exercise within the parameters errors, say with $F_\gamma = 9 \times 10^{-7}$ erg cm $^{-2}$, $z = 5.5$, Band energy indices $\beta = 2.5$, $\alpha = 1.7$ and $E_p = 70$ keV, produces a very reasonable $E_{p,i} = 455$ keV and $E_{\gamma,iso} = 9.3 \times 10^{52}$ erg. Following one of the latest GRB samples to test the Amati relation (Amati et al. 2008), this result places GRB 050502B right in the middle zone of the $E_{p,i}$ vs. $E_{\gamma,iso}$ plot validating sample. Note also that this energy corresponds to a typical GRB, being ~ 40 times smaller than the corresponding $E_{\gamma,iso}$ inferred for the extreme case of GRB 080916C (Abdo et al. 2009; Greiner et al. 2009), the most energetic GRB known to date.

Since the presence of a jet break suggests a conical GRB geometry, the true gamma-ray energy release, E_γ , is smaller than $E_{\gamma,iso}$, with $E_\gamma = f_b E_{\gamma,iso}$ (Frail et al. 2001; Sari et al. 1999). For the above choice of parameters, computing the beaming fraction, $f_b = 1 - \cos \theta$, with the $E_{\gamma,iso}$ corresponding newly calculated angle ($\theta \sim 3.2^\circ$), results in $E_\gamma = 1.45 \times 10^{50}$ erg. Two comments can be made at this point:

1) This rather low total energy suggests that the relatively large redshift of $z = 5.2$ cannot be overly large.

2) This value is smaller than the average of those reported in earlier surveys, clustering around the GRBs “standard” energy reservoir (e.g. Frail et al. 2001). As observed later by Ghirlanda et al. (2004) in more recent and larger GRB samples this clustering is in fact not so narrow, covering about 2 orders of magnitude.

Finally it would be interesting to see if GRB 050502B obeys the $E_{p,i} - E_\gamma$ Ghirlanda relation (Ghirlanda et al. 2004, 2007), but the large uncertainties in both the measured parameters and the model prevent a meaningful comparison.

5. Conclusions

As a main conclusion the data favor the high redshift nature of GRB 050502B. While even a very red color is not sufficient to claim a high redshift (see, e.g., GRB 060923A, GRB 070306), in this case an extra constraint is provided by β_{OX} being consistent with β_X . Also there is no significant excess N_H and furthermore the post-jet break slope α_X is consistent with α_{opt} , again favoring a single component origin for the two bands. The consistency of the time indices favors the other main conclusion: the existence of an achromatic jet break.

The scarcity of optical data limits a deeper discussion regarding the late engine model as an explanation for the X-ray giant flare and later activity (Falcone et al. 2006) and likewise in considering alternative models. It is interesting to note however, that the jet break appears after the end of the last bump, which could also be originated by later engine activity. No transition is observed from the shallow phase to a pre-jet break phase, likely because the extra “late prompt” component is added to the fireball model component. As the effects of the late engine activity cease, the afterglow shows then a standard jet break.

Given the high-redshift nature of GRB 050502B, its consequent afterglow red $R - I$ color and the fact that typical X-ray flares emit most of their flux in the γ -ray and X-ray bands (e.g. Page et al. 2007; Krühler et al. 2009), it is not very surprising that the simultaneous UVOT observation do not show evidence

for a strong rebrightening in the optical wavelength regime contemporaneous with the prominent X-ray flare.

Finally it is interesting to note that for $z = 5.2 \pm 0.3$, this would be one of the highest redshift observed achromatic breaks, when comparing with the samples of Liang et al. (2008) and Ghirlanda et al. (2007).

Acknowledgements. E.P. acknowledges financial support from contracts PRIN INAF 2006 and ASI I/088/06/0. The Dark Cosmology Centre is funded by the Danish National Research Foundation. T.K. acknowledges support by the DFG cluster of excellence “Origin and Structure of the Universe”. This work made use of data supplied by the UK Swift Science Data Centre at the University of Leicester. We thank G. Szokoly, D. Burlon and G. Ghirlanda for useful discussions and V. Sudilovski and K. Dzurella for improvements in the draft.

References

- Abdo, A. A., Ackermann, M., Arimoto, M., et al. 2009, *Science*, 323, 1688
 Amati, L., Frontera, F., Tavani, M., et al. 2002, *A&A*, 390, 81
 Amati, L., Guidorzi, C., Frontera, F., et al. 2008, *MNRAS*, 391, 577
 Arnaud, K. A. 1996, in *Astronomical Society of the Pacific Conference Series*, Vol. 101, *Astronomical Data Analysis Software and Systems V*, ed. G. H. Jacoby & J. Barnes, 17
 Band, D., Matteson, J., Ford, L., et al. 1993, *ApJ*, 413, 281
 Barthelmy, S. D., Barbier, L. M., Cummings, J. R., et al. 2005, *Space Science Reviews*, 120, 143
 Bhatt, B. C., Ramya, S., & Anupama, G. C. 2005, *GCN*, 3346
 Bolzonella, M., Miralles, J.-M., & Pelló, R. 2000, *A&A*, 363, 476
 Burrows, D. N., Hill, J. E., Nousek, J. A., et al. 2005a, *Space Science Reviews*, 120, 165
 Burrows, D. N., Romano, P., Falcone, A., et al. 2005b, *Science*, 309, 1833
 Cardelli, J. A., Clayton, G. C., & Mathis, J. S. 1989, *ApJ*, 345, 245
 Cenko, S. B., Fox, D. B., Rich, J., et al. 2005, *GCN*, 3358
 Chonis, T. S. & Gaskell, C. M. 2008, *AJ*, 135, 264
 Covino, S., D’Avanzo, P., Klotz, A., et al. 2008, *MNRAS*, 388, 347
 Cummings, J., Barbier, L., Barthelmy, S., et al. 2005, *GCN*, 3339
 Dickey, J. M. & Lockman, F. J. 1990, *ARA&A*, 28, 215
 Elíasdóttir, Á., Fynbo, J. P. U., Hjorth, J., et al. 2009, *ApJ*, 697, 1725
 Evans, P. A., Beardmore, A. P., Page, K. L., et al. 2007, *A&A*, 469, 379
 Falcone, A. D., Burrows, D. N., Lazzati, D., et al. 2006, *ApJ*, 641, 1010
 Frail, D. A., Kulkarni, S. R., Sari, R., et al. 2001, *ApJ*, 562, L55
 Fukugita, M., Shimasaku, K., & Ichikawa, T. 1995, *PASP*, 107, 945
 Galama, T. J. & Wijers, R. A. M. J. 2001, *ApJ*, 549, L209
 Gehrels, N., Chincarini, G., Giommi, P., et al. 2004, *ApJ*, 611, 1005
 Ghirlanda, G., Ghisellini, G., & Lazzati, D. 2004, *ApJ*, 616, 331
 Ghirlanda, G., Nava, L., Ghisellini, G., & Firmani, C. 2007, *A&A*, 466, 127
 Ghisellini, G., Nardini, M., Ghirlanda, G., & Celotti, A. 2009, *MNRAS*, 393, 253
 Greiner, J., Clemens, C., Krühler, T., et al. 2009, *A&A*, 498, 89
 Grupe, D., Nousek, J. A., vanden Berk, D. E., et al. 2007, *AJ*, 133, 2216
 Jakobsson, P., Fynbo, J. P. U., Ledoux, C., et al. 2006, *A&A*, 460, L13
 Jaunsen, A. O., Rol, E., Watson, D. J., et al. 2008, *ApJ*, 681, 453
 Kann, D. A., Klose, S., & Zeh, A. 2006, *ApJ*, 641, 993
 Krühler, T., Greiner, J., McBreen, S., et al. 2009, *ApJ*, 697, 758
 Krühler, T., Küpcü Yoldaş, A., Greiner, J., et al. 2008, *ApJ*, 685, 376
 Landolt, A. U. 1992, *AJ*, 104, 340
 Le Floc’h, E., Duc, P.-A., Mirabel, I. F., et al. 2003, *A&A*, 400, 499
 Liang, E.-W., Racusin, J. L., Zhang, B., Zhang, B.-B., & Burrows, D. N. 2008, *ApJ*, 675, 528
 Liang, E.-W., Zhang, B.-B., & Zhang, B. 2007, *ApJ*, 670, 565
 Malesani, D., Hjorth, J., Fynbo, J. P. U., et al. 2009, in *American Institute of Physics Conference Series*, Vol. 1111, *American Institute of Physics Conference Series*, ed. G. Giobbi, A. Tornambe, G. Raimondo, M. Limongi, L. A. Antonelli, N. Menci, & E. Brocato, 513–519
 Misra, K. & Pandey, S. B. 2005, *GCN*, 3350
 Nardini, M., Ghisellini, G., Ghirlanda, G., & Celotti, A. 2009, *ArXiv e-prints* 0734, accepted in *MNRAS*
 O’Donnell, J. E. 1994, *ApJ*, 422, 158
 Pagani, C., Falcone, A., Burrows, D. N., et al. 2005, *GCN*, 3333
 Page, K. L., Willingale, R., Osborne, J. P., et al. 2007, *ApJ*, 663, 1125
 Panaitescu, A. 2006, *Nuovo Cimento B Serie*, 121, 1099
 Predehl, P. & Schmitt, J. H. M. M. 1995, *A&A*, 293, 889
 Prochaska, J. X., Sheffer, Y., Perley, D. A., et al. 2009, *ApJ*, 691, L27
 Rhoads, J. E. 1997, *ApJ*, 487, L1
 Rich, J., Schmidt, B., & Christiansen, J. 2005a, *GCN*, 3338
 Rich, J., Schmidt, B., & Christiansen, J. 2005b, *GCN*, 3331

- Rol, E., van der Horst, A., Wiersema, K., et al. 2007, *ApJ*, 669, 1098
- Roming, P. W. A., Kennedy, T. E., Mason, K. O., et al. 2005, *Space Science Reviews*, 120, 95
- Roming, P. W. A., Koch, T. S., Oates, S. R., et al. 2009, *ApJ*, 690, 163
- Sakamoto, T., Barthelmy, S. D., Barbier, L., et al. 2008, *ApJS*, 175, 179
- Sakamoto, T., Sato, G., Barbier, L., et al. 2009, *ApJ*, 693, 922
- Sanchawala, K., Wu, W. L., Huang, K. Y., et al. 2005, *GCN*, 3334
- Sari, R., Piran, T., & Halpern, J. P. 1999, *ApJ*, 519, L17
- Sari, R., Piran, T., & Narayan, R. 1998, *ApJ*, 497, L17
- Sasaki, M., Manago, N., Noda, K., & Asaoka, Y. 2005, *GCN*, 3421
- Savaglio, S., Glazebrook, K., & LeBorgne, D. 2009, *ApJ*, 691, 182
- Schady, P., Falcone, A., Holland, S., et al. 2005, *GCN*, 3337
- Schady, P., Mason, K. O., Page, M. J., et al. 2007, *MNRAS*, 377, 273
- Schlegel, D. J., Finkbeiner, D. P., & Davis, M. 1998, *ApJ*, 500, 525
- Spergel, D. N., Verde, L., Peiris, H. V., et al. 2003, *ApJS*, 148, 175
- Stratta, G., Fiore, F., Antonelli, L. A., Piro, L., & De Pasquale, M. 2004, *ApJ*, 608, 846
- Tanvir, N. R., Levan, A. J., Rol, E., et al. 2008, *MNRAS*, 388, 1743
- Tody, D. 1993, in *Astronomical Society of the Pacific Conference Series*, Vol. 52, *Astronomical Data Analysis Software and Systems II*, ed. R. J. Hanisch, R. J. V. Brissenden, & J. Barnes, 173
- Torii, K. 2005, *GCN*, 4113
- Wainwright, C., Berger, E., & Penprase, B. E. 2007, *ApJ*, 657, 367
- Watson, D., Fynbo, J. P. U., Ledoux, C., et al. 2006, *ApJ*, 652, 1011
- Watson, D., Hjorth, J., Fynbo, J. P. U., et al. 2007, *ApJ*, 660, L101
- Zhang, B. & Mészáros, P. 2004, *International Journal of Modern Physics A*, 19, 2385